


REGULAR PAPER

# Adaptive sliding mode attitude control of quaternion model for aircraft based on neural network minimum parameter learning method

H.X. Zhuang 

College of Artificial Intelligence, Beijing Technology and Business University, Beijing 100048, China  
Email: [hxzhuang@btbu.edu.cn](mailto:hxzhuang@btbu.edu.cn)

**Received:** 28 November 2022; **Revised:** 29 March 2023; **Accepted:** 31 May 2023

**Keywords:** Sliding mode control; RBF network; Attitude control; Quaternion aircraft model; Actuator fault model

## Abstract

This paper studied the back-stepping adaptive sliding mode control (SMC) attitude problem of quaternion aircraft model based on radial basis function (RBF) network approximation. Firstly, a sliding mode controller is designed based on the back-stepping method (BSM) for the nonlinear aircraft model. Secondly, a RBF network algorithm is designed to compensate for the unknown and uncertain parts of the aircraft system. RBF network has simple network structure and good generalisation ability, avoids lengthy and unnecessary calculations, realises adaptive approximation of unknown parts in the aircraft model, and through the adjustment of adaptive weights, the convergence and stability of the entire closed-loop system (CLS) are guaranteed. Finally, the anti-interference performance of the controller is verified by simulation of the actuator fault model. Our proposed method has all-right control performance indicated by the simulation results.

## Nomenclature

### Abbreviation

AAC	aircraft attitude control
ACS	attitude control system
ADRC	active disturbance rejection control
AFS	actuator failure scenario
CLS	closed-loop system
BSM	back-stepping method
RBF	radial basis function
SMC	sliding mode control
TD	tracking differentiator
UAV	unmanned aerial vehicle

### Variables

$\chi$	heading angle
$\gamma$	flight path angle
$\mu$	velocity roll angle
$\psi$	yaw angle
$\theta$	pitch angle
$\phi$	roll angle
$\alpha$	angle-of-attack
$\beta$	sideslip angle

$D, L, Q$	drag, lift, and side forces, respectively
$g$	gravitational acceleration
$T_x$	thrust
$p, q, r$	angular velocity components
$\delta_a, \delta_r, \delta_e$	deflection angle vector of aileron, elevator, rudder
$\Delta\alpha, \Delta V$	perturbations from the trim values
$V_0$	trim velocity
$V$	velocity of aircraft
$C_l, C_m, C_n$	moment coefficients of roll, pitch and yaw, respectively
$S_r$	reference area
$\mathcal{L}$	reference lateral or longitudinal lengths
$I_x, I_y, I_z$	principal moments of inertia
$\rho$	air density
$M_a$	Mach number
$m$	aircraft mass
$x, y, z$	inertial position coordinates

## 1.0 Introduction

With the rapid development of aircraft technology and its application in the military field, the requirements of aircraft attitude control (AAC) are increasing, and it is urgent to improve the accuracy of attitude control. The research of aircraft related issues has attracted many scholars' interest, and the research of attitude control has also become a hot spot [1].

The war environment is becoming increasingly complex, and the new operational requirements and target characteristics have brought new problems and challenges to attitude control. The traditional control accuracy can no longer meet the requirements of future air combat. In order to improve the strike accuracy, enhance the self-defense performance, and meet the requirements of the rapidity and mobility of aircraft, it is very important to explore new attitude control methods.

Although there are still many technical problems and key theories to be solved in the practical application of aircraft, its application scope and mission in the field of production and life have been greatly expanded, such as disaster rescue, street view shooting, monitoring and patrol, electric power patrol, environmental protection detection, traffic monitoring, agricultural plant protection and so on. It is also expanding in the field and scope of military applications, such as regional search, theater communication support, strike effect evaluation, target guidance and other important combat tasks. In modern war, the confrontation between attack and defense is becoming increasingly fierce. Once the combat aircraft with important value is found by the enemy during the mission, it is likely to be regarded as an attack target by the enemy. In order to ensure that the aircraft can survive and continue to perform combat tasks when attacked by the enemy, the combat aircraft must have a sensitive, efficient and accurate attitude controller to automatically control the aircraft to avoid the enemy's attack. The agility and stability of aircraft has always been the primary issue of engineers' life cycle service from design, development to maintenance and operation. In the field of flight control, the focus of research is to constantly find new control technologies, and it is very important to improve the stability and agility of AAC, which has stimulated our enthusiasm and interest in the research of AAC.

### 1.1. Research status

There are many researches on attitude control of satellites [2, 3], reentry vehicle [4], missiles [5–7] and quadrotor [8]. Reference [2] proposed a new type of partial differential equation observer to explore the boundary attitude and vibration control of flexible satellites; Reference [4] proposes a new finite time attitude controller by introducing a non-singular finite time sliding mode manifold; Reference [3] applied the traditional  $H_1$  method and the  $H_1/LMI$  method of pole assignment considering parameter uncertainty to study the attitude control system (ACS) design of rigid flexible satellite with two vibration modes;

Reference [7] proposed a new attitude control method for nonlinear missile system, which combined the BSM with the linear active interference suppression control. Reference [8] studied the robust attitude control of a quadrotor aircraft under model mismatch and disturbance, and proposed an attitude control scheme based on dynamic inversion.

However, there are few researchers on AAC. For attitude control of nonlinear aircraft system, Reference [9] designed a robust flight control law based on BSM and active disturbance rejection control (ADRC). Reference [10] applies robust adaptive control and BSM to ACS of aircraft. Furthermore, the models they studied were all systems built in Euler coordinates. In general, we habitually use Euler angles (roll angle, pitch angle and yaw angle) to describe the attitude, but there are singularity points in using Euler angles to describe the attitude. The specific analysis is as follows:

Euler angle, direction cosine and quaternions are commonly used to describe the attitude angle, but Euler angle method has the problem of “singularity”, which can not calculate the attitude angle in all directions, such as the kinematic equation will become singular and induce no solutions when pitch angle  $\theta$  reaches  $90^\circ$ . The direction cosine method has a lot of trigonometry, quaternions can be introduced to solve the transformation problem, and the main advantages of this approach are less computing time, better accuracy and avoidance of the singularity problem.

If the mathematical model of the controlled object is known, the sliding mode controller can make the system output directly track the desired command, but the large modeling uncertainty requires a large switching gain, which causes chattering, which is an unavoidable problem in sliding mode control (SMC).

### 1.2. Research method

SMC combined with neural network approximation is used in the control of nonlinear systems. neural network is used to realise the adaptive approximation of the unknown part of the model, which can effectively reduce the fuzzy gain. The adaptive law of neural network is derived by Lyapunov method, and the stability and convergence of the whole closed-loop system (CLS) are guaranteed by adjusting the adaptive weight.

RBF neural network was proposed in 1988. Compared with multilayer feedforward BP network, the network has good generalisation ability, simple network structure, and avoids unnecessary and lengthy calculations. The research on RBF neural network shows that RBF neural network can approximate any nonlinear function under a compact set and any precision. At present, many research results of RBF neural network control for nonlinear systems have been published [11]; however, no scholars have applied RBF neural network algorithm combined with SMC to study AAC.

In this paper, the method of SMC combined with BSM is introduced into the MIMO system. For the typical MIMO nonlinear aircraft attitude control system, a SMC method based on RBF neural network is designed.

### 1.3. Research layout

The rest of this paper is structured as follows. Section 2 describes the non-linear aircraft model. Back-stepping adaptive SMC based on RBF network approximation design is designed in Section 3. The proof of asymptotic convergence and stability of the CLS is distributed in Section 4. Simulation results are presented in Section 5 to testify the effectiveness of the proposed control method. Finally, Section 6 concludes the paper.

## 2.0 Nonlinear aircraft model

Quaternion method is a more feasible method than Euler angle method, which avoids the singularity of Euler angular velocity equation when pitch angle  $\theta$  is equal to  $90^\circ$ . This method is also called Euler four parameter method [12]. The quaternion model has been derived in detail in reference [13]. For the convenience of readers, the derivation process of the model is described in detail as follows.

**Table 1.** The aerodynamic derivatives computed at the trim condition.

Aerodynamic derivative of rolling moment		
$l_q = \frac{1}{2} \rho V_0^2 S_r l_1 \frac{\partial C_l}{\partial q} / I_x$	$l_\beta = \frac{1}{2} \rho V_0^2 S_r l_1 \frac{\partial C_l}{\partial \beta} / I_x$	$l_r = \frac{1}{2} \rho_0^2 S_r l_1 \frac{\partial C_l}{\partial r} / I_x$
$l_{\beta\alpha} = \frac{1}{2} \rho V_0^2 S_r l_1 \frac{\partial C_l}{\partial \beta \alpha} / I_x$	$l_{r\alpha} = \frac{1}{2} \rho V_0^2 S_r l_1 \frac{\partial C_l}{\partial r \alpha} / I_x$	$l_p = \frac{1}{2} \rho V_0^2 S_r l_1 \frac{\partial C_l}{\partial p} / I_x$
$l_{\delta_r} = \frac{1}{2} \rho V_0^2 S_r l_1 \frac{\partial C_l}{\partial \delta_r} / I_x$	$l_{\delta_a} = \frac{1}{2} \rho V_0^2 S_r l_1 \frac{\partial C_l}{\partial \delta_a} / I_x$	
Aerodynamic derivatives of pitching moment		
$m_\alpha = \frac{1}{2} \rho V_0^2 S_r l_2 \frac{\partial C_m}{\partial \alpha} / I_y$	$m_q = \frac{1}{2} \rho V_0^2 S_r l_2 \frac{\partial C_m}{\partial q} / I_y$	$m_{\dot{\alpha}} = \frac{1}{2} \rho V_0^2 S_r l_2 \frac{\partial C_m}{\partial \dot{\alpha}} / I_y$
$m = \frac{1}{2} \rho V_0^2 S_r l_2 \frac{\partial C_m}{\partial V} / I_y$	$m_{\delta_e} = \frac{1}{2} \rho V_0^2 S_r l_2 \frac{\partial C_m}{\partial \delta_e} / I_y$	
Aerodynamic derivative of yaw moment		
$n_\beta = \frac{1}{2} \rho V_0^2 S_r l_3 \frac{\partial C_n}{\partial \beta} / I_z$	$n_r = \frac{1}{2} \rho V_0^2 S_r l_3 \frac{\partial C_n}{\partial r} / I_z$	$n_p = \frac{1}{2} \rho V_0^2 S_r l_3 \frac{\partial C_n}{\partial p} / I_z$
$n_{p\alpha} = \frac{1}{2} \rho V_0^2 S_r l_3 \frac{\partial C_n}{\partial p \alpha} / I_z$	$n_q = \frac{1}{2} \rho V_0^2 S_r l_3 \frac{\partial C_n}{\partial q} / I_z$	$n_{\delta_a} = \frac{1}{2} \rho V_0^2 S_r l_3 \frac{\partial C_n}{\partial \delta_a} / I_z$
$n_{\delta_r} = \frac{1}{2} \rho V_0^2 S_r l_3 \frac{\partial C_n}{\partial \delta_r} / I_z$		

We consider the vertical takeoff and dive aircraft system described by quaternions.

$$\begin{bmatrix} \dot{q}_0 \\ \dot{q}_1 \\ \dot{q}_2 \\ \dot{q}_3 \end{bmatrix} = \frac{1}{2} \begin{bmatrix} -q_1 & -q_2 & -q_3 \\ q_0 & -q_3 & q_2 \\ q_3 & q_0 & -q_1 \\ -q_2 & q_1 & q_0 \end{bmatrix} \begin{bmatrix} p \\ q \\ r \end{bmatrix} \tag{1}$$

$$\begin{bmatrix} \dot{p} \\ \dot{q} \\ \dot{r} \end{bmatrix} = \left( \frac{V}{V_0} \right)^2 + \begin{bmatrix} l_\beta \beta + l_q q + l_r r + (l_{\beta\alpha} \beta + l_{r\alpha}) \Delta \alpha \\ + l_p p + l_{\delta_a} \delta_a + l_{\delta_r} \delta_r \\ m_\alpha \Delta \alpha + m_q q - m_{\dot{\alpha}} p \beta \\ + m_v \Delta V + m_{\delta_e} \delta_e \\ + m_\alpha (g_0 / V) \times (\cos \theta \cos \varphi - \cos \theta_0) \\ n_\beta \beta + n_r r + n_p p + n_{p\alpha} p \Delta \alpha \\ + n_q q + n_{\delta_a} \delta_a + n_{\delta_r} \delta_r \end{bmatrix} + \begin{bmatrix} -i_1 \mathbf{qr} \\ i_2 \mathbf{pr} \\ -i_3 \mathbf{pq} \end{bmatrix} \tag{2}$$

where  $l_a = \frac{1}{2} \rho V_0^2 S_r l_1 \frac{\partial C_l}{\partial a} / I_x$ ,  $m_a = \frac{1}{2} \rho V_0^2 S_r l_2 \frac{\partial C_m}{\partial a} / I_y$ , and  $n_a = \frac{1}{2} \rho V_0^2 S_r l_3 \frac{\partial C_n}{\partial a} / I_z$  ( $a = \{\alpha, \beta, q, p, \dots\}$ ) and so on, the relationships between these variables are detailed in Table 1 of [10]. And  $i_1 = (I_z - I_y) / I_x$ ,  $i_2 = (I_z - I_x) / I_y$ , and  $i_3 = (I_y - I_x) / I_z$ . Here we introduce the factor  $(V/V_0)^2$  into rotational motion on account of these parameters are proportional to the square of velocity.

The unit-quaternion is a vector defined by  $[q_0 \ q_1 \ q_2 \ q_3]^T$  that satisfies  $q_0^2 + q_1^2 + q_2^2 + q_3^2 = 1$ . Unit quaternion provides a convenient mathematical notation for representing the orientation and

rotation of 3D objects. They are easier to compose than Euler angles and avoid the problem of gimbal locking. They are numerically more stable and possibly more efficient than rotation matrices.

**Assumption 1.** It is can be hypothesised that we can obtain the quaternion  $q$  and measure angular velocity  $[\mathbf{p} \ \mathbf{q} \ \mathbf{r}]^T$  in aircraft systems (1) and (2); and we need to measure the displacement components  $[x \ y \ z]^T$  and velocity  $V(V = \sqrt{V_x^2 + V_y^2 + V_z^2})$  in (1) and (2), and they are specifically contained in the following equation:

$$\begin{bmatrix} \dot{V}_x \\ \dot{V}_y \\ \dot{V}_z \end{bmatrix} = \begin{bmatrix} (T_x - D)/m - 2(q_0q_3 + q_1q_2)g \\ Q/m - [1 - 2(q_1^2 + q_3^2)]g \\ L/m - 2(q_2q_3 - q_0q_1)g \end{bmatrix} + \begin{bmatrix} 0 & \mathbf{r} & -\mathbf{q} \\ -\mathbf{r} & 0 & \mathbf{p} \\ \mathbf{q} & -\mathbf{p} & 0 \end{bmatrix} \begin{bmatrix} V_x \\ V_y \\ V_z \end{bmatrix} \tag{3}$$

After derivation, the coordinate transformation matrix from the airframe coordinate system to the inertial coordinate system determined by quaternion is

$$\begin{bmatrix} \dot{x} \\ \dot{y} \\ \dot{z} \end{bmatrix} = \begin{bmatrix} 1 - 2(q_2^2 + q_3^2) & 2(q_1q_2 - q_0q_3) & 2(q_1q_3 - q_0q_2) \\ 2(q_0q_3 - q_1q_2) & 1 - 2(q_1^2 + q_3^2) & 2(q_2q_3 - q_0q_1) \\ 2(q_1q_3 - q_0q_2) & 2(q_2q_3 - q_0q_1) & 1 - 2(q_1^2 - q_2^2) \end{bmatrix} \begin{bmatrix} V_x \\ V_y \\ V_z \end{bmatrix} \tag{4}$$

**Remark 1.** In Ref. [14], we can see more information of the attitude kinematic (1)–(2) and dynamic (3) and (4).

The aim of this paper is to resolve the problem of attitude tracking; it is the purpose of this paper to design a feedback controller which is bounded and satisfies  $\|q(t)\| = 1$  that enables the state of the CLS (1) and (2) to track the expected attitude motion  $q_r$ , which can be described in the following:

$$\begin{aligned} \lim_{t \rightarrow \infty} \xi(t) &= 0 \\ \xi(t) &= q(t) - q_r(t) \end{aligned} \tag{5}$$

and the deflection angle vector  $[\delta_a \ \delta_r \ \delta_e]^T$  is the control input.

For ease of description, we re-define the aircraft model as follow:

$$\begin{aligned} Y_1 &= [q_0 \ q_1 \ q_2 \ q_3]^T \\ Y_2 &= [\mathbf{p} \ \mathbf{q} \ \mathbf{r}]^T \\ Y_3 &= [x \ y \ z]^T \\ Y_4 &= [V_x \ V_y \ V_z]^T \\ U &\triangleq [\delta_a \ \delta_r \ \delta_e]^T \end{aligned} \tag{6}$$

Then we rewrite the aircraft model (1) and (2) as follow:

$$\begin{aligned} \dot{Y}_1 &= H_1(Y_1) Y_2 \\ \dot{Y}_2 &= H_2(Y_2) + H_3(Y_1, Y_2, Y_3, Y_4) + B(Y_1, Y_3, Y_4) U \end{aligned} \tag{7}$$

where

$$H_1(Y_1) = \frac{1}{2} \begin{bmatrix} -q_1 & -q_2 & -q_3 \\ q_0 & -q_3 & q_2 \\ q_3 & q_0 & -q_1 \\ -q_2 & q_1 & q_0 \end{bmatrix} \tag{8}$$

$$H_2(Y_2) = \begin{bmatrix} -(I_z - I_y) / I_x \mathbf{qr} \\ (I_z - I_x) / I_y \mathbf{pr} \\ -(I_y - I_x) / I_z \mathbf{pq} \end{bmatrix} \tag{9}$$

$$H_3(Y_1, Y_2, Y_3, Y_4) = \frac{1}{2} \rho V_0^2 S_r \mathcal{L} \times \left[ \begin{array}{c} \left[ \frac{\partial C_l}{\partial \beta} \beta + \frac{\partial C_l}{\partial q} q + \frac{\partial C_l}{\partial r} r \right. \\ \left. + \left( \frac{\partial C_l}{\partial \beta \alpha} \beta + \frac{\partial C_l}{\partial r \alpha} \right) \Delta \alpha + \frac{\partial C_l}{\partial p} p \right] / I_x \\ \hline \left\{ \frac{\partial C_m}{\partial \alpha} \Delta \alpha + \frac{\partial C_m}{\partial q} q - \frac{\partial C_m}{\partial \dot{\alpha}} p \beta + \frac{\partial C_m}{\partial V} \Delta V + \right. \\ \left. \frac{\partial C_m}{\partial \dot{\alpha}} (g_0 / V) \times (\cos \theta \cos \phi - \cos \theta_0) \right\} / I_y \\ \hline \left[ \frac{\partial C_n}{\partial \beta} \beta + \frac{\partial C_n}{\partial r} r + \frac{\partial C_n}{\partial p} p + \frac{\partial C_n}{\partial p \alpha} p \Delta \alpha + \frac{\partial C_n}{\partial q} q \right] / I_z \end{array} \right] \tag{10}$$

$$B(Y_1, Y_3, Y_4) = \frac{1}{2} \rho V_0^2 S_r \mathcal{L} \times \begin{bmatrix} \frac{\partial C_l}{\partial \delta_a} / I_x & \frac{\partial C_l}{\partial \delta_r} / I_x & 0 \\ 0 & 0 & \frac{\partial C_m}{\partial \delta_e} / I_y \\ \frac{\partial C_n}{\partial \delta_a} / I_z & \frac{\partial C_n}{\partial \delta_r} / I_z & 0 \end{bmatrix} \tag{11}$$

It can be clearly seen from the above formula that many uncertain factors are involved in the whole system. For example, the atmospheric moment coefficient  $\frac{\partial C_l}{\partial *}$ ,  $\frac{\partial C_m}{\partial *}$  and  $\frac{\partial C_n}{\partial *}$  depends on the change of Mach number  $M_a$ . The Mach number  $M_a$  is related to the state variable. During the actual flight of the aircraft, it is difficult to determine these atmospheric moment coefficients, which leads to the uncertainty of the aircraft model. Therefore, because of the uncertainty of the atmospheric moment coefficient  $\frac{\partial C_l}{\partial *}$ ,  $\frac{\partial C_m}{\partial *}$  and  $\frac{\partial C_n}{\partial *}$ ,  $H_3$  and  $B$  are unknown, which makes the control design more complex, and the system structure (7) is particularly difficult [15].

In order to settle this puzzle, we introduce a new variable  $F(t)$  as follow

$$F(t) = H_3(Y_1, Y_2, Y_3, Y_4) + B(Y_1, Y_3, Y_4) U - B_0 U \tag{12}$$

where  $B_0$  is defined as

$$B_0 = \frac{1}{2} \rho V_0^2 S_r \mathcal{L} \Phi|_{M_a=const} \tag{13}$$

where  $\Phi|_{M_a=const}$  is defined as

$$\Phi|_{M_a=const} = \begin{bmatrix} \frac{\partial C_l}{\partial \delta_a} / I_x & \frac{\partial C_l}{\partial \delta_r} / I_x & 0 \\ 0 & 0 & \frac{\partial C_m}{\partial \delta_e} / I_y \\ \frac{\partial C_n}{\partial \delta_a} / I_z & \frac{\partial C_n}{\partial \delta_r} / I_z & 0 \end{bmatrix} \Big|_{M_a=const}$$

We can obtain the coefficients  $\frac{\partial C_l}{\partial \delta_a}$ ,  $\frac{\partial C_l}{\partial \delta_r}$ ,  $\frac{\partial C_m}{\partial \delta_e}$ ,  $\frac{\partial C_n}{\partial \delta_a}$ , and  $\frac{\partial C_n}{\partial \delta_r}$  by selecting the appropriate constant Maher number  $M_a$ . These coefficients are part of  $B_0$ , and decompose the uncertain part into variable  $F(t)$ . Thus, the dynamic uncertainty existing in (7) can be reduced to the total uncertainty  $F(t)$ , hence, the complicity of control design is also reduced. Therefore, we can rewrite the system (7) as follow:

$$\dot{Y}_1 = H_1(Y_1) Y_2 \tag{14a}$$

$$\dot{Y}_2 = H_2(Y_2) + F(t) + B_0 U(t) \tag{14b}$$

**Remark 2.** In order to reduce the complexity of control design, by introducing new state variables  $F(t)$ , the aircraft system (7) can be simplified to a second-order system. However,  $F(t)$  is also unknown due to the lack of information of  $Y_3$  and  $Y_4$ , and  $F(t)$  is considered as an uncertain term containing information of  $Y_3$  and  $Y_4$ .

To proceed the controller design and stability proof, the following lemmas are given.

**Lemma 1.** [16] Let  $f, V: [0, \infty) \rightarrow \mathbb{R}$ . Then

$$\dot{V} \leq -\alpha V + f, \quad \forall t \geq t_0 \geq 0$$

implies that

$$V(t) \leq e^{-\alpha(t-t_0)} V(t_0) + \int_{t_0}^t e^{-\alpha(t-\tau)} f(\tau) d\tau, \quad \forall t \geq t_0 \geq 0$$

for any finite constant  $\alpha$ .

**Lemma 2.** [17] The linear tracking differentiator is considered as follow:

$$\begin{cases} \dot{\chi}_1 = \chi_2 \\ \dot{\chi}_2 = -\kappa_1 R^2 (\chi_1 - Y_r) - \kappa_2 R \chi_2 \end{cases} \tag{15}$$

where  $\kappa_1 > 0$  and  $\kappa_2 > 0$  are constants, and  $R > 0$  is the tuning parameter.

Suppose that  $\kappa_1 > 0, \kappa_2 > 0$  and  $Y_r : [0, \infty) \rightarrow R$  is a function satisfying  $\sup_{t \in [0, \infty)} (|Y_r| + |\dot{Y}_r|) = M_1 < \infty$  for constant  $M_1 > 0$ . Then the linear tracking differentiator (15) is convergent in the sense that, for  $\forall a > 0$ ,

$$\begin{cases} \lim_{R \rightarrow \infty} |\chi_1 - Y_r| = 0 \\ \lim_{R \rightarrow \infty} |\chi_2 - \dot{Y}_r| = 0 \end{cases}$$

uniformly for  $t \in [a, \infty)$ .

**Lemma 3.** [18] The slope of the saturation function,  $\text{sat}\left(\frac{s}{\Phi |\eta|}\right)$ , increases as the approach angle magnitude,  $|\eta|$ , decreases; hence,

$$\lim_{|\eta| \rightarrow 0} \text{sat}\left(\frac{s}{\Phi |\eta|}\right) = \text{sign}(s)$$

### 3.0 Back-stepping adaptive smc based on rbf network approximation design

#### 3.1.1 Back-stepping procedure

Next, we will design the BSM of the system (14): first, let's define some variables, as shown in Table 2. Next, we start with the definition of state error  $z_1$

$$z_1 = Y_1 - Y_{r,1}$$

where the reference value of  $Y_r$  is  $Y_{r,1}$ , next, take the derivative of  $z_1$ , and we get

$$\dot{z}_1 = \dot{Y}_1 - \dot{Y}_r = H_1(Y_1) Y_2 - \dot{Y}_r \tag{16}$$

**Table 2.** The variable definition in BSM

Actual state	Desired state	State error	Relationship between variables
$Y_i$	$Y_{r,i}$	$z$	$z = Y_i - Y_{r,i}$

Based on the principle of BSM,  $Y_2$  is regarded as the virtual control input, used for applying the following dynamic expectations

$$\dot{z}_1 = -\Lambda z_1 = -\text{diag}[\lambda_1 \quad \lambda_2 \quad \lambda_3 \quad \lambda_4] z_1 \quad (17)$$

To ensure the asymptotic stability of (17), the design matrix  $\Lambda$  is chosen as  $\lambda_i > 0$ ,  $i = 1, 2, 3, 4$ . Therefore, combining (16) with (17), we can get the solution

$$Y_{r,2} = H_{1L}^{-1}(Y_1) (\dot{Y}_r - \Lambda z_1) \quad (18)$$

where the left inverse matrix of  $H_1(Y_1)$  is denoted by  $H_{1L}^{-1}(Y_1)$ .

**Remark 3.** In (8),  $H_1(Y_1)$  has four  $\mathbf{R}^{3 \times 3}$  subdeterminants.  $q_0, q_1, q_2$  and  $q_3$  are respectively the values of these subdeterminants. The column rank of  $H_1(Y_1)$  is reduced if and only if  $q_0 = q_1 = q_2 = q_3 = 0$ , otherwise, if any  $q_i$  satisfies  $q_i \neq 0$ , then the column rank of  $H_1(Y_1)$  is full. Note  $q_0^2 + q_1^2 + q_2^2 + q_3^2 = 1$ ,  $q_0 = q_1 = q_2 = q_3 = 0$  cannot happen at the same time. Hence  $H_1(Y_1)$  is full column rank, which means the existence of the left inverse matrix of  $H_1(Y_1)$  [5].

### 3.2. RBF network approximation

For the sake of overcoming the interference inside the system and obtain the accurate modeling information  $F(t)$  of the controlled object, fractional order SMC and BSM based on RBF network approximation should be combined.

Then, we design the sliding mode surface (SMS) as follow:

$$s = z_2 \quad (19)$$

Next, consider the following reaching law

$$\dot{s} = -\Pi s - \Sigma \text{sign}^\zeta(s) \quad (20a)$$

$$\Pi = \text{diag}[\pi_1 \quad \pi_2 \quad \pi_3], \pi_i > 0 \quad (20b)$$

$$\Sigma = \text{diag}[\sigma_1 \quad \sigma_2 \quad \sigma_3], \sigma_i > 0 \quad (20c)$$

where  $\text{sign}^\zeta(s) = [\text{sign}(s_1) |s_1|^\zeta, \text{sign}(s_2) |s_2|^\zeta, \text{sign}(s_3) |s_3|^\zeta]$  with  $0 < \zeta < 1$ .

Taking the derivative of  $s$ , and combining the reaching law (20a), we get

$$\begin{aligned} \dot{s} &= H_2(Y_2) + F(t) + B_0 U(t) - \dot{Y}_{r,2} \\ &= -\Pi s - \Sigma \text{sign}^\zeta(s) \end{aligned} \quad (21)$$

we can acquire the control law by solving for  $U(t)$  in equality (21)

$$U(t) = B_0^{-1} (-\Pi s - \Sigma \text{sign}^\zeta(s) - H_2(Y_2) - F(t) + \dot{Y}_{r,2}) \quad (22)$$

Note that, the controller (25) contains the uncertainty  $F(t)$ , which is partially unknown to us; Therefore, it cannot be directly applied to the actual system before obtaining  $F(t)$ . Next, we need to utilise the RBF NN to approximate  $F(t)$ .



The uncertainty  $F(t)$  is approximated adaptively by RBF NN. The RBF NN algorithm is:

$$R_j = \exp\left(-\frac{\|\mathbf{t} - c_j\|^2}{2b_j^2}\right), \quad j = 1, 2, \dots, m$$

$$F(t) = \mathbf{WR}(t) + \varepsilon \tag{23}$$

where  $\mathbf{t}$  is input signal of network;  $j$  is the number of hidden layer nodes in the network;  $c_j$  is the center of the basis function;  $b_j$  is the width of the Gaussian function of the  $j$ th hidden layer unit;  $\mathbf{R} = [r_1, r_2, \dots, r_m]^T$  is the output of the Gaussian function;  $\mathbf{W} \in R^{3 \times m}$  is the ideal neural network weights;  $\varepsilon$  is the approximation error of neural network,  $\varepsilon = [\varepsilon_1, \varepsilon_2, \varepsilon_3]^T$ ,  $|\varepsilon_i| \leq \varepsilon_N$ .

$F(t)$  is approximated by the RBF NN, and the output of RBF NN is

$$\hat{F}(t) = \hat{\mathbf{W}}\mathbf{R}(t) \tag{24}$$

where,  $\hat{F}(t)$  is the approximation of the RBF NN. We adopt the NN minimum parameter learning method, let  $\varphi = \|\mathbf{W}\|^2$ ,  $\varphi > 0$ , the estimation of  $\varphi$  is  $\hat{\varphi}$ ,  $\tilde{\varphi} = \hat{\varphi} - \varphi$ .

**Remark 4.** In the actual control system design, for guaranteeing that the input value of the NN is a Gaussian basis function (GBF) within the valid range, the coordinate vector  $c_j$  of the center point of the GBF should be determined according to the actual range of the network input value. In order to ensure the effective mapping of the GBF, the width  $b_j$  of the GBF needs to be taken as an appropriate value. By proving the stability of the closed-loop Lyapunov function, the adjustment of  $\hat{W}$  is designed.

Using adaptive RBF NN to approximate the total uncertainty of  $F(t)$ , the controller (22) is rewritten as

$$U(t) = B_0^{-1} \left( -\Pi s - \Sigma \text{sign}^s(s) - H_2(Y_2) - \frac{1}{2}s\hat{\varphi}\mathbf{R}^T\mathbf{R} + \dot{Y}_{r,2} \right) \tag{25}$$

**4.0 Main results**

**Theorem 1.** Consider the subsystem (14a), and SMS given by (19). If the RBF neural network algorithm and control law are respectively established as (23) and (25), then the plant trajectories asymptotically converge into a small region of SMS, and the global asymptotic stability of the CLS (14b) is guaranteed within a finite reaching time by defining the adaptive control laws:

$$\dot{\hat{\varphi}} = \frac{\rho}{2} \|s\|^2 \mathbf{R}^T \mathbf{R} - \kappa \rho \hat{\varphi} \tag{26}$$

where  $\kappa > 0$ .

*Proof.* A Lyapunov function candidate is defined

$$L = \frac{1}{2} + \frac{1}{2\rho} \tilde{\varphi}^2 \tag{27}$$

where  $\rho > 0$ .

With (21) and (25), the derivative of  $L$  can be calculated by

$$\begin{aligned} \dot{L} &= s\dot{s} + \frac{1}{\rho} \tilde{\varphi} \dot{\hat{\varphi}} \\ &= s \left( \mathbf{WR} + \varepsilon - \Pi s - \Sigma \text{sign}^s(s) - \frac{1}{2}s\hat{\varphi}\mathbf{R}^T\mathbf{R} \right) + \frac{1}{\rho} \tilde{\varphi} \dot{\hat{\varphi}} \\ &\leq \frac{1}{2} \|s\|^2 \varphi \mathbf{R}^T \mathbf{R} + \frac{1}{2} - \frac{1}{2} \|s\|^2 \hat{\varphi} \mathbf{R}^T \mathbf{R} + \|\varepsilon\| \|s\| - \|\Sigma\| \|s\| + \frac{1}{\rho} \tilde{\varphi} \dot{\hat{\varphi}} - \|\Pi\| \|s\|^2 \\ &= -\frac{1}{2} \|s\|^2 \tilde{\varphi} \mathbf{R}^T \mathbf{R} + \frac{1}{2} + \|\varepsilon\| \|s\| - \|\Sigma\| \|s\| + \frac{1}{\rho} \tilde{\varphi} \dot{\hat{\varphi}} - \Pi s^2 \end{aligned}$$

$$\begin{aligned}
 &= \tilde{\varphi} \left( -\frac{1}{2} \|s\|^2 \mathbf{R}^T \mathbf{R} + \frac{1}{\rho} \dot{\hat{\varphi}} \right) + \frac{1}{2} + \|\varepsilon\| \|s\| \\
 &- \|\Sigma\| \|s\| - \|\Pi\| \|s\|^2 \\
 &\leq \tilde{\varphi} \left( -\frac{1}{2} \|s\|^2 \mathbf{R}^T \mathbf{R} + \frac{1}{\rho} \dot{\hat{\varphi}} \right) + \frac{1}{2} - \|\Pi\| \|s\|^2
 \end{aligned} \tag{28}$$

Substituting the adaptive control law (26) into equation (28), it can be acquired

$$\begin{aligned}
 \dot{L} &\leq -\kappa \tilde{\varphi} \hat{\varphi} + \frac{1}{2} - \Pi s^2 \\
 &\leq -\frac{\kappa}{2} (\tilde{\varphi}^2 - \varphi^2) + \frac{1}{2} - \Pi s^2 \\
 &= -\frac{\kappa}{2} \tilde{\varphi}^2 - \Pi s^2 + \frac{1}{2} (\kappa \varphi^2 + 1)
 \end{aligned} \tag{29}$$

Let  $\kappa = \frac{2 \|\Pi\|}{\rho}$ , next, we get

$$\begin{aligned}
 \dot{L} &\leq -\frac{\|\Pi\|}{\rho} \tilde{\varphi}^2 - \|\Pi\| s^2 + \left( \frac{\kappa}{2} \varphi^2 + \frac{1}{2} \right) \\
 &= -2 \|\Pi\| \left( \frac{1}{2\rho} \tilde{\varphi}^2 + \frac{1}{2} s^2 \right) + \left( \frac{\kappa}{2} \varphi^2 + \frac{1}{2} \right) \\
 &= -2 \|\Pi\| L + Q
 \end{aligned} \tag{30}$$

where  $Q = \frac{\kappa}{2} \varphi^2 + \frac{1}{2}$ .

According to Lemma 1, solve inequality (30), it can be obtained

$$L \leq \frac{Q}{2 \|\Pi\|} + \left( L(0) - \frac{Q}{2 \|\Pi\|} \right) e^{-2\|\Pi\|t} \tag{31}$$

namely,

$$\begin{aligned}
 \lim_{t \rightarrow \infty} L &= \frac{Q}{2 \|\Pi\|} = \frac{\frac{\kappa}{2} \varphi^2 + \frac{1}{2}}{2 \|\Pi\|} = \frac{\kappa \varphi^2 + 1}{4 \|\Pi\|} \\
 &= \frac{\frac{2\|\Pi\|}{\rho} \varphi^2 + 1}{4 \|\Pi\|} = \frac{\varphi^2}{2\rho} + \frac{1}{4 \|\Pi\|}
 \end{aligned} \tag{32}$$

Substituting (32) into Equation (30), it can be getted

$$\dot{L} \leq -2 \|\Pi\| L + Q = 0 \tag{33}$$

Hence, the state trajectory of the CLS (14b) is asymptotically stable under the application of the controller (25). □

**Remark 5.** Two conclusions are used in the proof of the Theorem 1. (i) When the first unequal-sign in (27) inequality is reduced, this conclusion is applied:  $s^2 \varphi R^T R + 1 = s^2 \|W\|^2 R^T R + 1 = s^2 \|W\|^2 \|R\|^2 + 1 = s^2 \|W^T R\|^2 + 1 \geq 2sW^T R$ , namely,  $sW^T R \leq \frac{1}{2} s^2 \varphi R^T R + \frac{1}{2}$ . (ii) When the second unequal-sign in (29) inequality is reduced, this conclusion is applied: because  $(\tilde{\varphi} + \varphi)^2 \geq 0$ , then,  $\tilde{\varphi}^2 + 2\tilde{\varphi}\varphi + \varphi^2 \geq 0$ ,  $\tilde{\varphi}^2 + 2\tilde{\varphi}(\hat{\varphi} - \tilde{\varphi}) + \varphi^2 \geq 0$ , namely,  $2\tilde{\varphi}\hat{\varphi} \geq \tilde{\varphi}^2 - \varphi^2$ .

**Theorem 2.** Research the CLS (14b) with sliding mode surface (19). If the controller was designed as (22), the tracking errors  $z_1$  and  $z_2$  of the system will converge to a small residual set of the origin in a finite time and stay there for the rest of the time.

*Proof.* The proof process is divided into two steps.

Step 1: According to (17), the selection of  $\Lambda$  is based on the principle of back-stepping, Lyapunov functional is chosen as follows:

$$V_1 = \frac{1}{2}z_1^2 \tag{34}$$

Then

$$\dot{V}_1 = z_1\dot{z}_1 = -\sum_{i=1}^4 \lambda_i z_{1i}^2 - z_1^T H_1(Y_1) z_2 \tag{35}$$

by selecting positive  $\lambda_i$  large enough, we obtain  $\dot{V}_1 < 0$  when  $V_1$  is out of a certain bounded region.

Step 2: Choosing the Lyapunov function as follows

$$V_2 = \frac{1}{2}z_2^2 \tag{36}$$

The time derivative of Lyapunov function (36) is

$$\dot{V}_2 = z_2^T \dot{z}_2 \tag{37}$$

With (21) and (25), the derivative of  $V_2$  can be calculated by

$$\begin{aligned} \dot{V}_2 &= s \left( WR + \varepsilon - \Pi s - \Sigma \text{sign}^\varepsilon(s) - \frac{1}{2} s \hat{\varphi}^T \mathbf{R} \right) \\ &\leq \frac{1}{2} \|s\|^2 \varphi^T \mathbf{R} + \frac{1}{2} - \frac{1}{2} \|s\|^2 \hat{\varphi}^T \mathbf{R} + \|\varepsilon\| \|s\| - \|\Sigma\| \|s\| - \|\Pi\| \|s\|^2 \\ &= -\frac{1}{2} \|s\|^2 \tilde{\varphi}^T \mathbf{R} + \frac{1}{2} + \|\varepsilon\| \|s\| - \|\Sigma\| \|s\| - \Pi s^2 \\ &\leq -\frac{1}{2} \|s\|^2 \tilde{\varphi}^T \mathbf{R} + \frac{1}{2} - \|\Pi\| \|s\|^2 \end{aligned} \tag{38}$$

Next, scaling down  $\dot{V}_2$ , it can be acquired

$$\begin{aligned} \dot{V}_2 &< -\frac{1}{2} \|s\|^2 \tilde{\varphi}^T \mathbf{R} + \frac{1}{\rho} \tilde{\varphi} \dot{\hat{\varphi}} + \frac{1}{2} - \|\Pi\| \|s\|^2 \\ &\leq \tilde{\varphi} \left( -\frac{1}{2} \|s\|^2 \mathbf{R}^T \mathbf{R} + \frac{1}{\rho} \dot{\hat{\varphi}} \right) + \frac{1}{2} - \|\Pi\| \|s\|^2 \end{aligned} \tag{39}$$

According to Theorem 1, we know  $\dot{V}_2 < \dot{L} \leq 0$ , hence, it can be obtained

$$\dot{V}_2 < 0 \tag{40}$$

In conclusion, define Lyapunov function  $V = V_1 + V_2$ ,  $\dot{V} = \dot{V}_1 + \dot{V}_2 < 0$ .

Hence, the tracking errors  $z_1$  and  $z_2$  are driven by the controller (25) to converge to the neighbourhood of the origin and remain there for all subsequent times.  $\square$

**Remark 6.** We can acquire the virtual control input  $Y_{r,2}$  by calculating (18), but  $\dot{Y}_r$  may not be acquired without difficulty because of the complex structure of  $H_{1L}^{-1}(Y_1)$ . Here, the tracking differentiator (TD) [5] is introduced so as to obtain the  $\dot{Y}_r$ . Here's a brief design of TD which is applied to track reference signal.

$$\begin{cases} \dot{\chi}_1 = \chi_2 \\ \dot{\chi}_2 = -\kappa_1 R^2 (\chi_1 - Y_r) - \kappa_2 R \chi_2 \end{cases} \tag{41}$$

where  $\chi_1$  and  $\chi_2$  are the state variables of TD,  $\kappa_1 > 0, \kappa_2 > 0$  are constants that denote the maximum actuation available in the system; and  $R > 0$  is the tuning parameter.

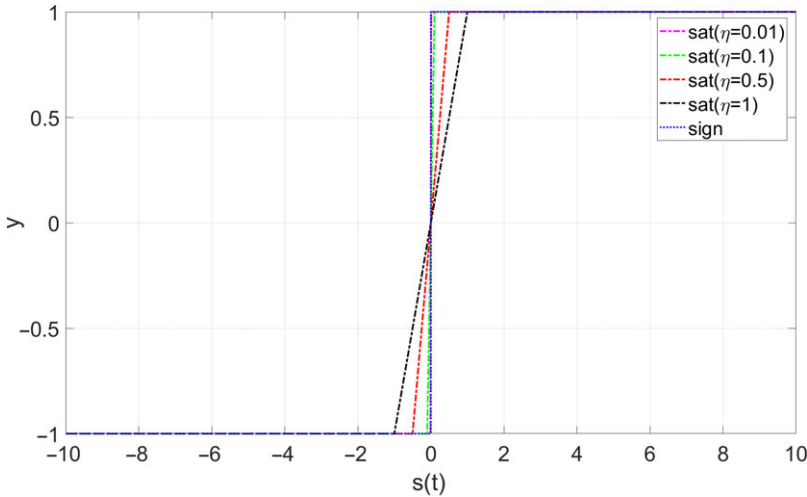


**Figure 1.** Comparison of saturation function and switching function.

In the light of Lemma 2, the TD states  $\chi_1, \chi_2$  will be approximate to  $Y_r, \dot{Y}_r$ , respectively as fast as possible. Xia, Y.Q. etc. have proved the advantages of this tracking method, for more details, please refer to Refs [5, 6]. See Ref. [19] for further explanation of TD. Thus  $\dot{Y}_r$  can be gotten with the help of designing of TD for  $Y_r$ .

**Remark 7.** In theory, we give an analysis to prove the stability of the CLS, which at least shows that this method is theoretically feasible. However, SMC has a disadvantage, that is, chattering caused by switching functions cannot be eliminated. For this reason, we use the saturation function  $\text{sat}\left(\frac{s}{\Phi|\eta|}\right)$  instead of the switching function  $\text{sign}(s)$  to weaken the chattering generated by the switching function. According to Lemma 3, we know that  $\lim_{|\eta| \rightarrow 0} \text{sat}\left(\frac{s}{\Phi|\eta|}\right) = \text{sign}(s)$ . The specific theoretical proof and analysis are detailed in the literature [18], we won't repeat it here. In fact, it can be seen from Fig. 1 that as  $\eta$  gets smaller, the saturation function gets closer to the switching function. Hence, the controller can be rewritten as

$$\hat{U}(t) = B_0^{-1} \left( -\Pi s - \Sigma \text{sat}\left(\frac{s}{\Phi|\eta|}\right)^{\zeta} - H_2(Y_2) - \hat{F}(t) + \dot{Y}_{r,2} \right) \tag{42}$$

**5.0 Simulation results and discussion**

To demonstrate the validity and effectiveness of the proposed method in this paper, it was applied the Airbus-300 aircraft model [20]. See Table 3 for specific flight conditions and data.

It can be seen from the Sections 3 and 4 that the convergence speed of the state trajectory can be adjusted by these parameters  $\Pi, \Sigma, \zeta$ , which can be tuned to weaken the chattering on the sliding surface according to Ref. [10]. Table 4 shows the simulation parameters, which are selected by basis of the theorem and remark in the paper. That is to say, the controller (42) can make the system track converge to the predetermined SMS with fast speed and accurate response in the presence of uncertainty and disturbance, and maintained there for all subsequent time.

It is hypothesised that the desired quaternion is as follows

$$q_r = [q_{0,r} \quad q_{1,r} \quad q_{2,r} \quad q_{3,r}]^T = [0.7\sin(t) \quad \cos(t) \quad 2\sin(t) \quad \cos(t)]^T \tag{43}$$

and the initial attitude orientation of the aircraft is the same as in Ref. [21], which is  $q(0) = [0.3 \quad 0.2 \quad -0.3 \quad 0.8832]^T$ .

**Table 3.** The aerodynamic derivatives computed at the trim condition.

Geometric parameters of Airbus-300			
Symbol	Value	Symbol	Value
$h/m$	600	$Ma$	0.228
$V_0/(m/s)$	77	$m/kg$	$1.3 \times 10^5$
$I_x/(kg \cdot m^2)$	$6.011 \times 10^6$	$I_y/(kg \cdot m^2)$	$10.53 \times 10^6$
$I_z/(kg \cdot m^2)$	$15.73 \times 10^6$	$I_{xz}/(kg \cdot m^2)$	$0.330 \times 10^6$
$S/(m^2)$	260	$b/m$	44.84
$\rho/(kg \cdot m^3)$	1.156	$\bar{c}/(m)$	6.60

Small derivative of Airbus-300's longitudinal motion			
$\alpha_0/(^\circ)$	7.84	$C_{D\alpha}/rad^{-1}$	0.814
$\delta_s/(^\circ)$	0	$C_{DMA}$	3.0698
$(C_L)_0$	1.417	$C_{D\delta_e}$	0.0623
$(C_D)_0$	0.163	$C_{m\delta_e}/rad^{-1}$	-1.688
$C_{L\alpha}/rad^{-1}$	5.66	$C_{m\dot{\alpha}}/s$	-10.42
$C_{L\dot{\alpha}}/rad^{-1}$	1.00	$C_{mMa}/s$	0.4937
$C_{LM}$	0.7166	$C_{mq}/s$	-27.22
$C_{L\delta_e}/ra^{-1}$	0.433	$C_{ma}/rad^{-1}$	-1.203
$(C_m)_0$	-0.0356	$C_{Lq}$	3.20
$(\frac{\partial T}{\partial V})_0$	0	$(\frac{\partial T}{\partial \delta_p})_0$	80,261.8

Small derivative of Airbus-300's lateral motion			
$C_{Y\beta}/rad^{-1}$	-1.09	$C_{l\delta_a}/rad^{-1}$	-0.1315
$C_{Y\delta_a}/rad^{-1}$	0	$C_{l\delta_r}/rad^{-1}$	0.0473
$C_{Y\delta_r}/rad^{-1}$	0.253	$C_{n\beta}/rad^{-1}$	0.5315
$C_{l\beta}/rad^{-1}$	-0.716	$C_{nr}/s$	-3.18
$C_{lp}/s$	-4.54	$C_{nr}/s$	-0.36
$C_{lr}/s$	4.695	$C_{n\delta_a}/rad^{-1}$	-0.0255
$C_{Yp}/rad^{-1}$	2.349	$C_{n\delta_r}/rad^{-1}$	-0.477
$C_{Yr}/rad^{-1}$	2.23		

Datas from: Rudolf B., Wolfgang A., Robert L., Flugregelung, Springer, Berlin, 2011.

**Table 4.** Parameter value of simulation

Parameter	Value	Parameter	Value
$\Sigma$	diag[ 15 15 15 ]	$\rho$	0.05
$\Pi$	diag[ 30 30 30 ]	$\zeta$	0.5
$c_j$	[ -2 -1 0 1 2 ]	$b_j$	3

The attitude history for state  $_0$  is shown in the top graph of Fig. 2. Similar curves for  $q_1, q_2$  and  $q_3$  are achieved as well. The attitude quaternion tracking errors converges to zero as shown in the Fig. 3, which shows that the controller (42) achieves high-precision performance on the attitude stabilisation in the presence of uncertainties and disturbances. It is clear that the proposed aircraft control system can ensure that the attitude quaternions effectively track the commanded quaternions by choosing a reasonable positive parameter  $\Lambda = 0.6I_3$ , where  $I_3$  is the  $\mathbb{R}^{3 \times 3}$  identity matrix. The control deflection angles is illustrated in the Fig. 4.

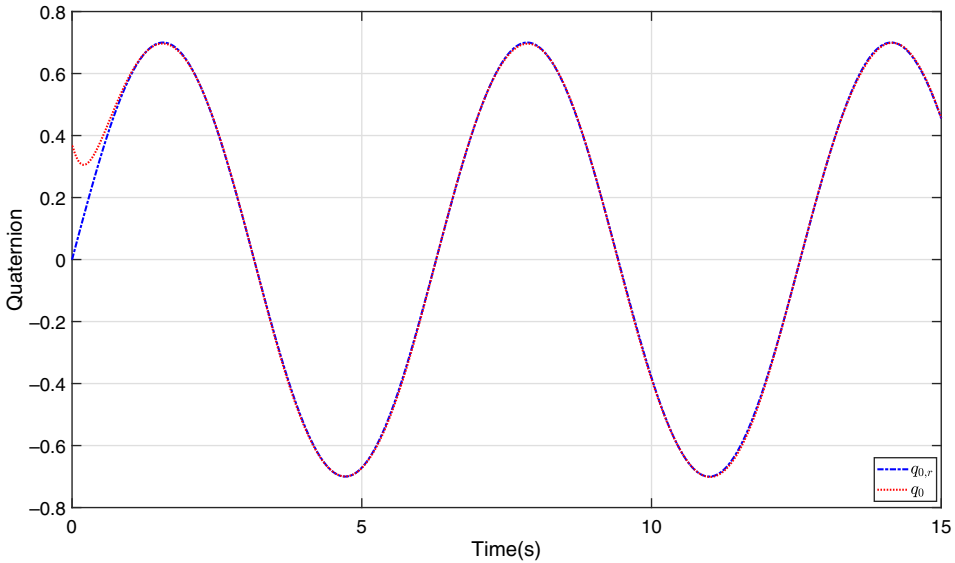


Figure 2. Profiles of the attitude.

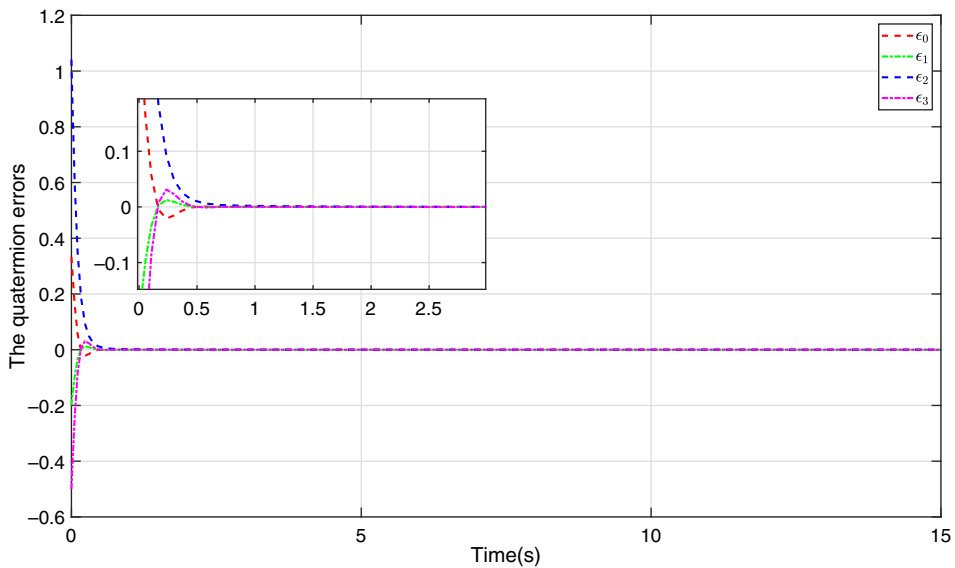


Figure 3. The quaternion errors.

The sliding surface function parameters and corresponding approximated parameters are chosen in Table 4. As shown in Fig. 5, the sliding surface function reaches the reachable state of  $s_i = 0, i = 1, 2, 3$  in 4s, and stays there all the time, which proves that the sliding surface selected in this paper is very ideal. It is clear that quickly approximates to  $F(t)$  in Fig. 6.

We introduce the actuator fault scenario (AFS) as follow in order to further illustrate the performance of the designed controller.

$$\dot{Y}_1 = H_1(Y_1) Y_2, \tag{44a}$$

$$\dot{Y}_2 = H_2(Y_2) + F(t) + B_0 \Delta \hat{U}(t). \tag{44b}$$

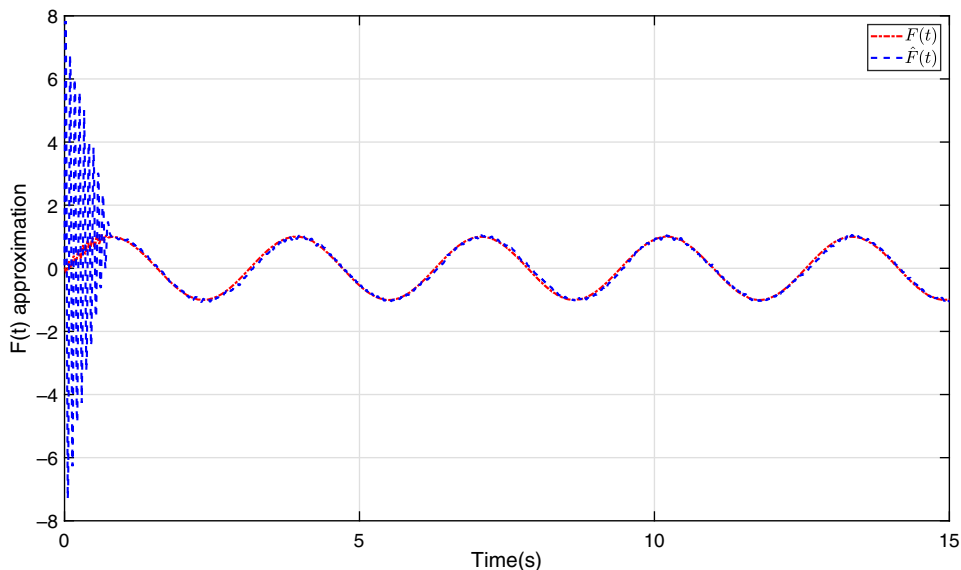


Figure 4.  $F(t)$  and approximation.

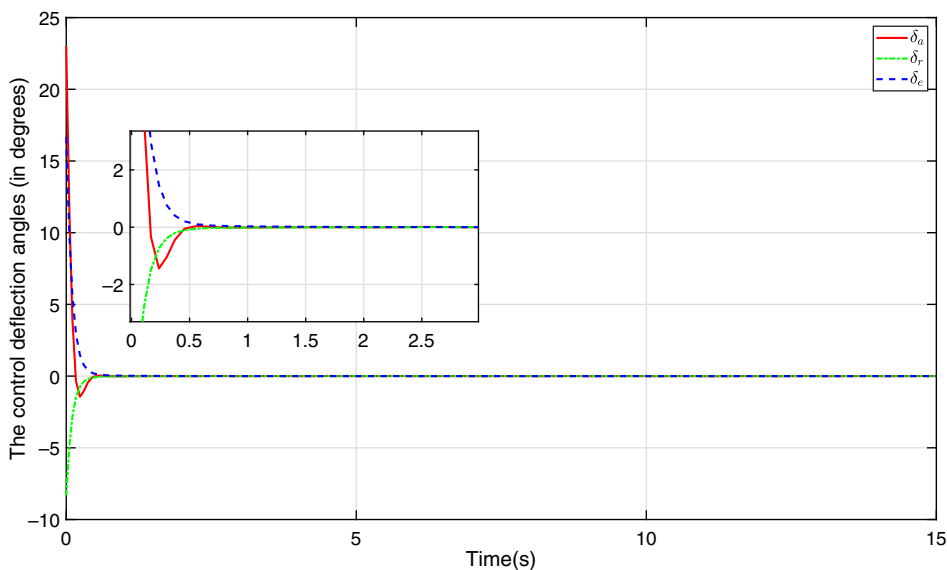


Figure 5. The control deflection angles (in degrees).

where  $\Delta = \text{diag}(\delta_1, \delta_2, \delta_3)$  is the actuator effectiveness, which satisfies  $0 < \delta_i \leq 1, i = 1, 2, 3$ . Note that the case  $\delta_i(t) = 1$  means that the  $i$ th actuator works normally, and  $0 < \delta_i < 1$  corresponds to the case in which the  $i$ th actuator has partially lost its effectiveness, but it still works.

We define an AFS  $\Delta = \text{diag}(\delta_1, \delta_2, \delta_3)$  as follows so as to further illustrate the performance of the designed controller (42)

$$\delta_i(t) = \begin{cases} 1, & \text{if } t < 5s \\ 0.3 + 0.1\sin(0.5t + i\pi/3), & \text{if } t \geq 5s \end{cases} \quad (45)$$

As shown in Fig. 7, the simulation experiment of the tracking errors in the AFS. It is set at 5s that the actuator fails, and there is a slight overshoot and chattering at 5s. The state response trajectory also

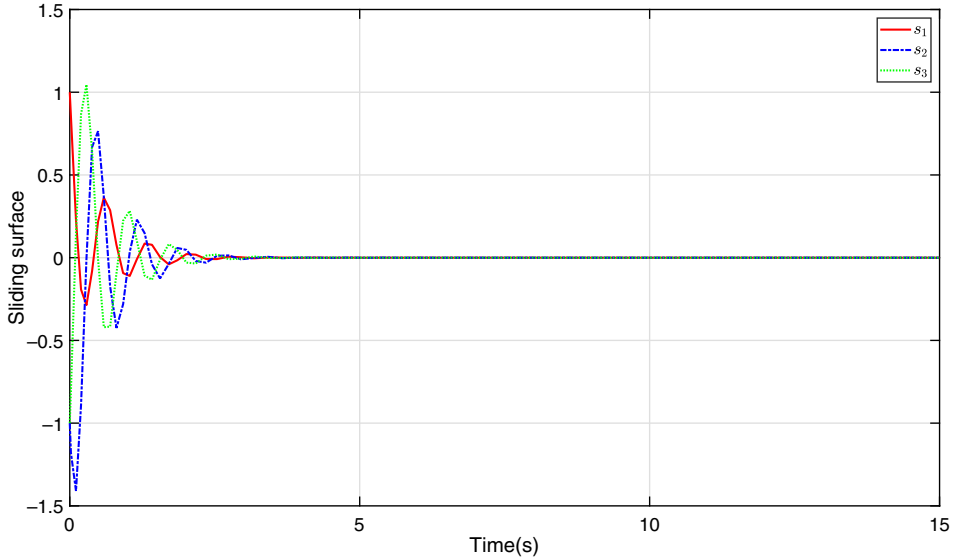


**Figure 6.** The sliding surface.

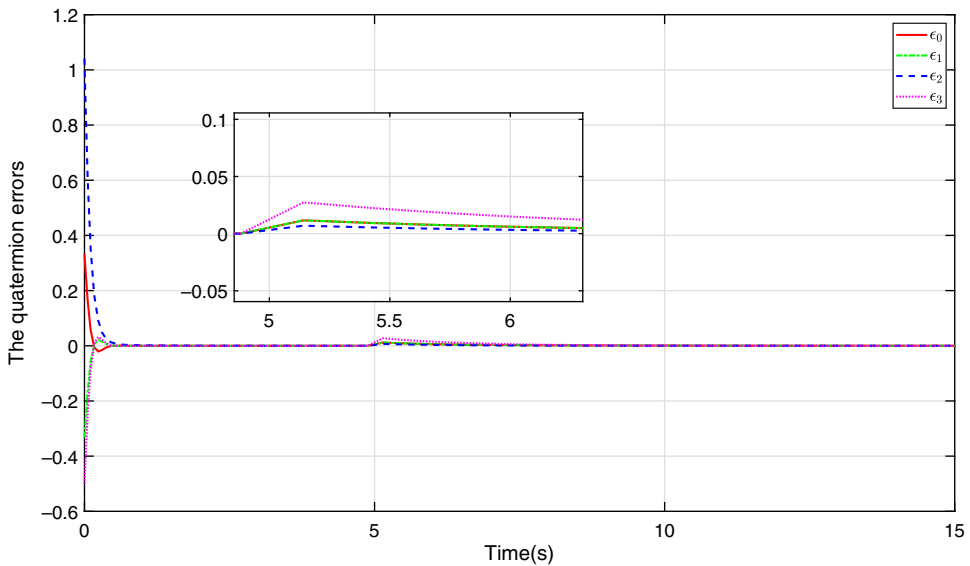


**Figure 7.** The quaternion errors.

fluctuates slightly, but it stabilises within 3s. It proves that the controller not only has good stability, but also has strong robustness and anti-interference.

Compared with Fig. 4, the control signal under the AFS has a slight step at 5s and can be driven into the region of the SMS, which is shown in Fig. 8

- (i) From the dynamic convergence process of the system, the robustness and stability of the proposed controller are obvious;
- (ii) From the convergence rate and convergence trend of the state trajectory, the convergence speed is fast;



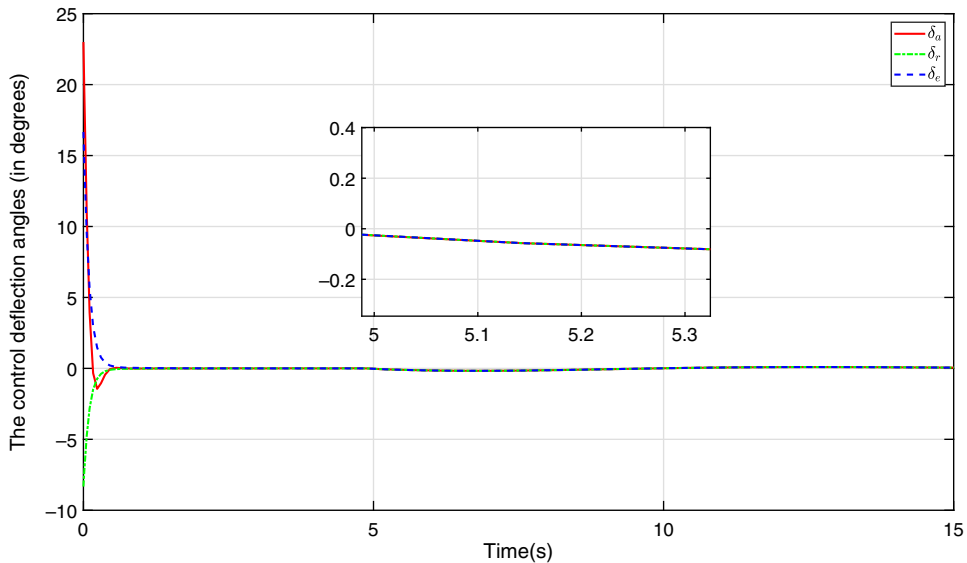


**Figure 8.** The control deflection angles (in degrees).

- (iii) From Figs 7 and 8, even in the case of AFS, the controller still has strong stability and robustness. Although the state trajectory fluctuates slightly near zero at 3s, it becomes stable instantly.

## 6.0 Conclusions

In this paper, we applied the adaptive SMC based on RBF NN approximation combining with BSM to investigate the AAC under the quaternion model. First, the quaternion model of the six degree of freedom nonlinear aircraft was transformed. And then a sliding mode surface function was established. Next, a sliding mode controller was designed, which improved the accuracy and robustness of the system. The uncertain term  $F(t)$  is approximated by RBF NN method and the differential term  $\dot{Y}_r$  was estimated by TD technique. In the simulation experiment, the actuator fault scenario was set up, which proved the feasibility of the proposed method.

**Acknowledgements.** The authors would like to thank the editors and reviewers for their valuable and helpful comments, which have improved the presentation.

**Funding.** This work was prepared at the College of Artificial Intelligence, Beijing Technology and Business University and was supported by the Start up fund for young teachers' scientific research of Beijing Technology and Business University (Grant No.19008023128).

**Declaration of conflicting interests.** No potential conflict of interest was reported by the authors. No conflict of interest exists in the submission of this manuscript, and manuscript is approved by all authors for publication.

## References

- [1] Tian, B., Liu, L., Lu, H., Zuo, Z., Zong, Q. and Zhang, Y. Multivariable finite time attitude control for quadrotor UAV: theory and experimentation, *IEEE Trans. Ind. Electron.*, 2017, **65**, (3), pp 2567–2577.
- [2] Ataei, M.M., Salarieh, H., Pishkenari, H.N. and Jalili, H. Boundary control design based on partial differential equation observer for vibration suppression and attitude control of flexible satellites with multi-section solar panels, *J. Vibr. Control*, 2021, **0**, (0), pp 1–11.
- [3] Souza, A. and Souza, L. Comparison of the satellite attitude control system design using the  $H_\infty$  method and  $H_\infty/MIL$ . with pole allocation considering the parametric uncertainty *WSEAS Trans. Circ. Syst.*, 2021, **20**, pp 88–95.

- [4] Jie, G., Sheng, Y. and Liu, X. Finite-time sliding mode attitude control for a reentry vehicle with blended aerodynamic surfaces and a reaction control system. *Chin. J. Aeronaut.*, 2014, **27**, (4), pp 964–976.
- [5] Xia, Y., Shi, P., Liu, G., Rees, D. and Han, J. Active disturbance rejection control for uncertain multivariable systems with time-delay. *IET Control Theory Appl.*, 2007, **1**, (1), pp 75–81.
- [6] Xia, Y., Zhu, Z. and Fu, M. Back-stepping sliding mode control for missile systems based on an extended state observer. *IET Control Theory Appl.*, 2011, **5**, (1), pp 93–102.
- [7] Zhuang, H., Sun, Q., Chen, Z. and Zeng, X. Active disturbance rejection control for attitude control of missile systems based on back-stepping method. *Int. J. Control Automat. Syst.*, 2021, **19**, (11), pp 3642–3656.
- [8] Wang, Z., Zhao, J., Cai, Z., Wang, Y. and Liu, N. Onboard actuator model-based incremental nonlinear dynamic inversion for quadrotor attitude control: method and application. *Chin. J. Aeronaut.*, 2021, **34**, (11), pp 216–227.
- [9] Zhuang, H., Sun, Q., Chen, Z. and Zeng, X. Back-stepping active disturbance rejection control for attitude control of aircraft systems based on extended state observer. *Int. J. Control Automat. Syst.*, 2021, **19**, (6), pp 2134–2149.
- [10] Zhuang, H., Sun, Q., Chen, Z. and Zeng, X. Robust adaptive sliding mode attitude control of aircraft systems based on back-stepping method. *Aerosp. Sci. Technol.*, 2021, **118**, pp 1–18.
- [11] Park, J. and Sandberg, I. Universal approximation using radial basis function networks. *Neural Computat.*, 2012, **3**, (2), pp 246–257.
- [12] Pamadi, B.N. Performance, Stability, Dynamics, and Control of Airplane, 2nd Edition, Institute of Aeronautics and Astronautics, American, 2013.
- [13] Zhuang, H., Zhang, X., Sun, Q. and Chen, Z. Fuzzy adaptive sliding mode attitude control of quaternion model for aircraft based on back-stepping method. *Data Driven Control and Learning Systems Conference*, May, 2023, Xiangtan, China.
- [14] Yuan, Z. and Qian, X. *Control Flight Mechanics and Computer Simulation*, Beijing, China: National Defense Industry Press, 2001.
- [15] Xia, Y., Lu, K., Zhu, Z. and Fu, M. Adaptive back-stepping sliding mode attitude control of missile systems. *International Journal of Robust and Nonlinear Control*, 2013, **23**, (15), pp 1699–1717.
- [16] Ioannou, P.A. and Sun, J. Robust Adaptive Control, 1st ed. PTR Prentice-Hall, 1995.
- [17] Guo, B. and Zhao, Z. Active Disturbance Rejection Control for Nonlinear Systems: An Introduction, John Wiley & Sons, Singapore Pte. Ltd, 2016.
- [18] Buckholtz, K.R. Approach angle-based switching function for sliding mode control design. *Proceedings of the American Control Conference Anchorage*, 8–10 May, 2002, pp 2368–2373.
- [19] Han, J. From PID to active disturbance rejection control. *IEEE Trans. Ind. Electron.*, 2009, **56**, (3), pp 900–906.
- [20] Liu, S. Flight Dynamics and Control of Modern Aircrafts, 1st edition, Shanghai Jiaotong University Press, Shanghai, China, 2014.
- [21] Chen, Z. and Huang, J. Attitude tracking and disturbance rejection of rigid spacecraft by adaptive control. *IEEE Trans. Automat. Control*, 2009, **54**, (3), pp 600–605.